Using Lagrangian coherent structures to analyze fluid mixing by cilia

Sarah Lukens,[1,a)] Xingzhou Yang,[2,b)] and Lisa Fauci[1,c)]
[1]*Department of Mathematics, Tulane University, 6823 St. Charles Avenue, New Orleans, Louisiana 70118, USA*
[2]*Department of Mathematics & Statistics, and Center for Computational Sciences, Mississippi State University, Mississippi State, Mississippi 39762, USA*

(Received 17 September 2009; accepted 10 November 2009; published online 5 January 2010)

Motivated by the desire to understand the fluid flow within the airway surface liquid of the lung, we consider the flow generated by a computational model of a motile, internally actuated cilium. The cilium, along with a mucus layer modeled by linear elastic elements, is coupled to a viscous, incompressible fluid. The evolution of this coupled system is captured using an immersed boundary method. The Eulerian velocity field computed on a grid is used to compute finite-time Lyapunov exponent fields, whose maximal ridges identify Lagrangian coherent structures (LCSs). The computed LCS uncovers a barrier that separates a recirculation region of fluid that remains near the beating cilium from fluid that is advected downstream. Moreover, periodic stretching and folding of this region gives rise to complex mixing. Flow structures around a cilium propelling a mucus layer are compared to flow structures around a cilium with no mucus load. © *2010 American Institute of Physics*. [doi:10.1063/1.3271340]

In the human body, cilia have been identified on almost all cells, including embryonic, kidney, and brain cells.[14] Some cilia serve sensory functions, and other motile cilia act to generate flows. Recently, it has been demonstrated that motile cilia of airway epithelia are also chemosensory.[27] Fluid flow generated by beating cilia transports mucus layers in the respiratory tract and a fertilized ovum in the oviduct. This flow can also convey important chemical or mechanical signals. For instance, the unidirectional flow generated by rotating nodal cilia in the embryonic node is responsible for determination of left-right asymmetry in development of many vertebrates.[17] It is, therefore, of fundamental interest to analyze flow structures generated by ciliary beating. These flow structures can identify what regions of fluid near the cilium and epithelia remain nearby as the cilium beats, what regions eventually get advected, and the extent of stirring or mixing in the fluid. Here, we use modern methods in computational fluid dynamics, along with a dynamical system approach, to identify Lagrangian coherent structures in the flow generated by a computational model of a motile cilium. We use these computed structures to uncover a recirculation region of fluid that remains near the beating cilium and show that periodic stretching and folding of this region gives rise to complex mixing.

I. INTRODUCTION

Motile cilia are hairlike appendages that project from a cell's surface and beat to move fluid or to transport the cell. Identical to eucaryotic flagella, cilia are shorter and occur in larger groups. Ciliated protists rely on the coordinated beating of arrays of cilia for propulsion and planktotrophic larvae capture small planktonic food with bands of cilia.[30] Physiologically, these appendages are also responsible for ovum transport in the oviduct, cerebrospinal fluid movement in the brain, and transport of mucus across respiratory epithelia.[1,15,29,31] The fluid in the periciliary layer of the airway surface liquid in the lungs, where the respiratory cilia beat, shields the epithelial cell surface from the mucus layer and is thought to be of key importance in lung defense.[11] The leftward flow generated by rotating nodal cilia in some vertebrates determines left-right asymmetry in developing embryos, since when the flow direction is reversed by imposing an artificial flow, the left-right decision is reversed.[13,17,18,24] While it is not yet established whether the signal transduction mechanism at work here is chemical or mechanical, the flow features around the cilia and the epithelium in the node certainly play a role in the process. Besides being of fundamental interest in cell biology and physiology, there has recently been a surge of interest in flows generated by cilia and flagella, as synthetic microswimmers are being designed for possible use in drug delivery and microsurgery and to enhance mixing in microfluidic devices.[8,10]

A cilium, while beating tens of times per second, has a length on the order of 30–50 μm. At this spatiotemporal scale, viscous forces dominate inertial forces, and the fluid dynamics are well described by the Stokes equations. Most importantly, in this low Reynolds number regime, the sequence of shapes traced out by the beating cilium cannot be time reversible for net fluid motion or swimming to occur.[23] A cilium beats by first progressing through a power stroke, where it is held fairly straight and pushes fluid forward, returning to its original position in a recovery stroke, where it bends closer to the cell boundary [see Fig. 1(a)]. This ciliary beatform is governed by an elaborate internal structure, the axoneme, that is powered by dynein molecular motors distributed regularly along its length and circumference. Typi-

[a)]Electronic mail: slukens@math.tulane.edu.
[b)]Electronic mail: XYang@math.msstate.edu.
[c)]Electronic mail: fauci@tulane.edu.

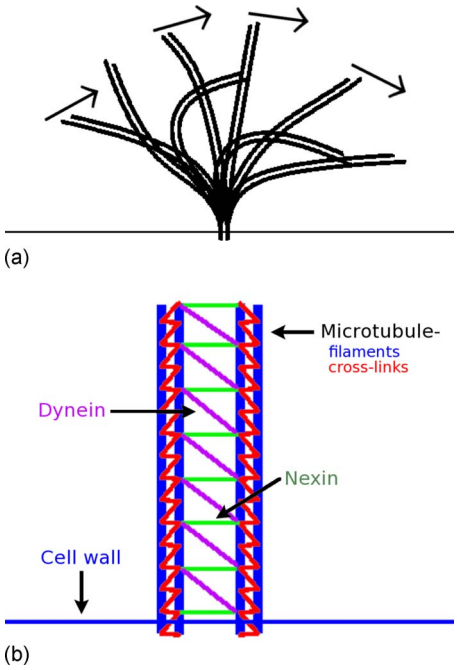

FIG. 1. (Color online) (a) Superimposed snapshots of a model cilium at eight frames within a typical beat. The arrows indicate when the cilium is in the power stroke, beating toward the right. Note that the computational cilium consists of two microtubules with dynein motors regularly spaced between them. These dyneins generate forces that cause relative sliding of the microtubules. (b) A schematic of the two-microtubule axoneme, depicting the structural springs that comprise the microtubules, the structural springs that model nexin links, and the location of the dynein motors (see Ref. 4 for details).

cally, a circular cross section of the "9+2" axoneme consists of a central pair of singlet microtubules surrounded by nine outer doublet microtubules and encased by the cell membrane.[16,34] Nodal cilia, while still motile, lack the central pair (9+0). The bending of the axoneme is caused by sliding between pairs of outer doublets due to the action of the dynein motors. While the local force production of the individual dyneins is translated into the regular beating of the global structure, the precise nature of the spatial and temporal control mechanisms regulating the various flagellar and ciliary beats is still unknown.[3,12]

The coupling of an internally actuated, elastic body (the cilium) with a viscous, incompressible fluid is a classic example of fluid-structure interactions in biological fluid dynamics. The beatform and frequency of the ciliary beat cycle is an emergent property of this complex, coupled mechanical system. In this paper, we investigate the flow features around a computational model of a cilium that incorporates discrete representations of dynein motors along with the passive elastic structure of the axoneme.[4,5,35] Although this two-dimensional (2D) model employs a reduced axonemal structure [see Fig. 1(b)], the curvature-controlled dynein activation dynamics can produce realistic ciliary beats when coupled with an accurate fluid solver.[4] This framework has been used to examine how fluid viscosity influences the model cilium's beat frequency and has demonstrated that hydrodynamic coupling leads to phase locking of neighboring model cilia.[35] Moreover, the propulsion of a mucus layer by the model cilium has also been examined.[6]

Flow structures around swimming organisms at both high and moderate Reynolds numbers have been successfully identified using Lagrangian analysis, based upon velocity fields measured from both laboratory experiments and computational models.[20,21,33] Here, we use the velocity field data computed around a single model cilium propelling an elastic mucus layer to identify Lagrangian coherent structures (LCSs), ridges of the finite-time Lyapunov exponent (FTLE) field.[9,25] We find a well-defined LCS that separates fluid advected by the cilium from fluid that remains in a recirculation region near the cilium. With the knowledge of the LCS, we examine the trajectories of groups of tracer particles and demonstrate that a high level of fluid mixing, reminiscent of a Smale horseshoe map,[32] occurs within the cilium-mucus layer.

II. METHODOLOGY

A. Fluid-structure interaction

Our coupled fluid-cilium-mucus computational model uses an immersed boundary formulation. The details of this model may be found in Refs. 4–6 and 35. The Navier–Stokes equations which govern the fluid are

$$\rho\left[\frac{\partial \mathbf{u}}{\partial t}+\mathbf{u}\cdot\nabla\mathbf{u}\right]=-\nabla p+\mu\Delta\mathbf{u}+\mathbf{F}(\mathbf{x},t), \tag{1}$$

$$\nabla\cdot\mathbf{u}=0, \tag{2}$$

where ρ is the fluid density, μ is the fluid viscosity, t is time, $\mathbf{u}$ is the fluid velocity, p denotes the pressure, and $\mathbf{F}$ is the force density which is exerted on the fluid by the axoneme and cell wall.

This immersed boundary formulation provides a framework for coupling the dynamics of passive and actuated flexible boundaries with a surrounding viscous, incompressible fluid.[22] As shown above, elastic structures are accounted for by suitable contributions to the force term $\mathbf{F}$ in the fluid dynamics equations. This force is a Dirac delta function layer of force that is supported only by the region of fluid that coincides with material points of the structures. Once these forces are accounted for, using a discretized delta function,[22] the fluid equations may be solved efficiently on a regular background grid. Here, we use a uniform finite difference grid, with periodic boundary conditions and solve the fluid equations using a FFT-based method that is first order in time and second order in space.[7] Once the fluid equations are solved, the positions of the immersed structures are updated using the computed velocity field.

The 2D model cilium consists of two microtubules [see Fig. 1(b)], built by an array of cross-linked linear springs, that give rise to a structure that is highly resistant to stretching and compression, as well as bending. Dynein motors are represented as dynamic elastic linkages between the microtubules that contract when activated, thus imparting force. These links may form, change connectivity, and may be broken during the course of the simulation. In addition to the

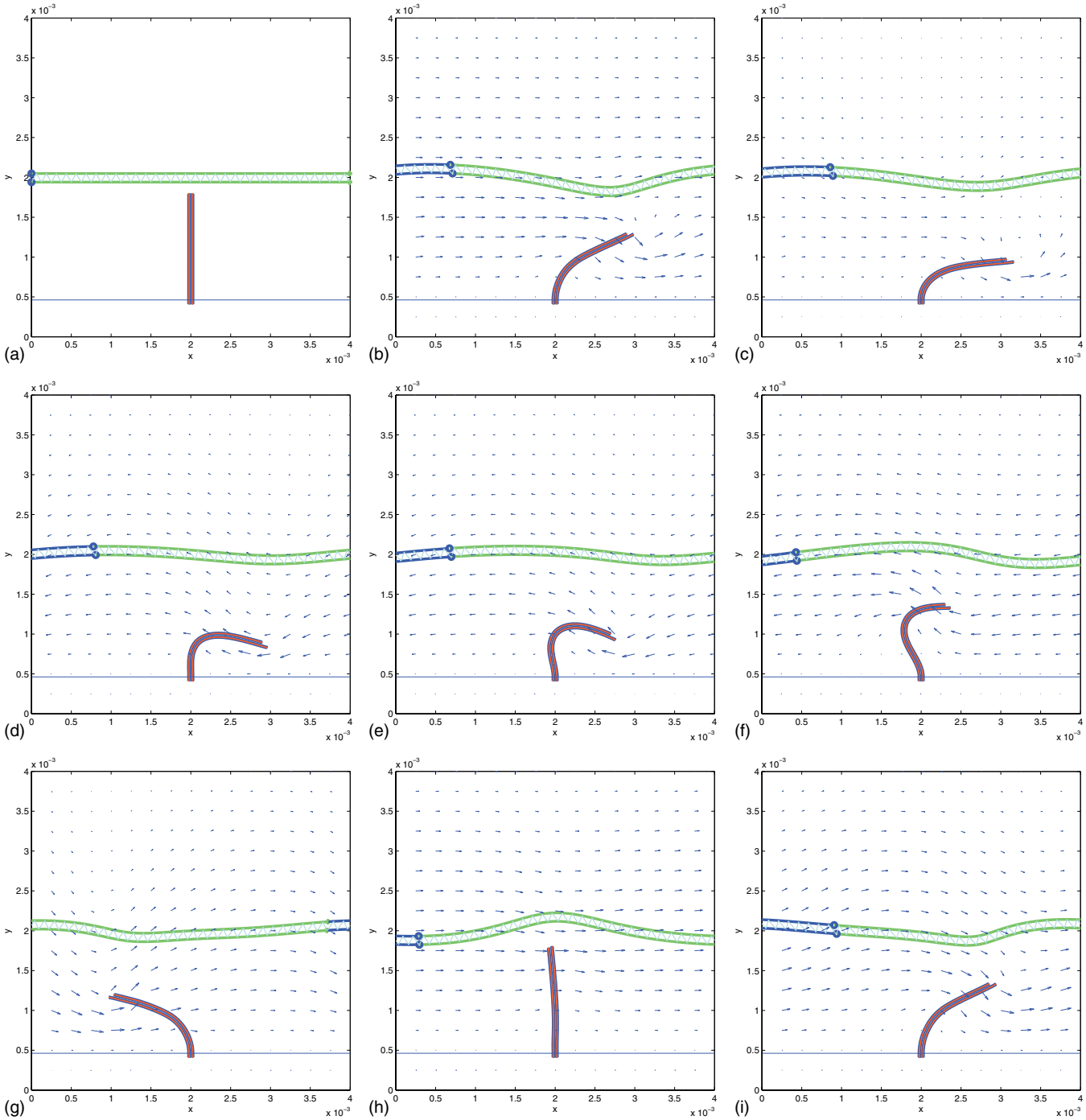

FIG. 2. (Color) Snapshots of velocity fields around a model cilium (14 μm in length) and elastic mucus layer at different times during 1.1 beat cycle. The beat frequency is approximately 35 Hz, and the power stroke accounts for about 30% of the beat cycle. Note that periodic boundary conditions are used for the fluid as well as the mucus layer. The blue dots on the mucus layer mark material points that illustrate the net forward transport of the layer by the cilium. The computed mucus transport speed is approximately 98 μm/s.

cilium, we include a discrete representation of a mucus layer that is modeled by cross-linked fibers, each built by linear springs. We illustrate the results of a typical simulation in Fig. 2. Each frame in Fig. 2 shows the full computational domain, where periodic boundary conditions were imposed on the fluid velocity and pressure in both the horizontal and vertical directions. This series of snapshots shows the evolution of the ciliary beat, the fluid velocity field, and the position of the (periodic) mucus layer. The geometry of the beat is not preset, but emerges from the coupling of the passive elastic properties of the microtubules and the mucus layer, the dynein activation kinetics, and the viscous fluid. Moreover, neither the beat frequency nor the durations of the power or recovery stroke within the beat are preset, but arise as a result of a geometric switch.[4] The basic idea of this switch is to monitor the amount of sliding or shear that has taken place between the two microtubules during either the power or recovery stroke. Once this sliding has reached a maximum threshold, the phase of the cilium switches from power to recovery stroke, or vice versa.

Motivated by the desire to understand the extent of fluid mixing in the periciliary layer of the air surface liquid in the lungs, we examine, even in this simplified case, the flow features near the beating cilium. Experiments by Matsui *et al.*[15] on tracheobroncial epithelial cell cultures have exhibited that the entire periciliary liquid is transported in a uniform manner at the same rate as the mucus layer. However, previous theoretical studies have predicted that only a modest transport of liquid occurs in the periciliary layer, compared to mucus transport.[2] For an overview of current models of mucociliary clearance, along with a discussion of their merits, limitations, and links to experiments, we refer the reader to a recent review article by Smith *et al.*[29] We note that an important feature of our model is that the elastic mucus layer need not remain flat, but experiences deformations due to the fluid coupling.

B. Identifying LCS

The immersed boundary method is built upon a Lagrangian description of the immersed elastic structures, an Eulerian description of the fluid velocity field, and a grid-dependent discrete delta function to communicate between these descriptions.[22] Unsteady flow features have been traditionally analyzed using the Eulerian velocity field. Here, we use the computed Eulerian velocity field to construct the FTLE field, whose maximal ridges (LCS) identify transport barriers in the flow and tend to material lines for long integration times.[25]

The Eulerian fluid velocity field $\mathbf{u}$ is related to the flow map,

$$\phi_{t_0}^{t_0+T_I}(\mathbf{x}):\mathbf{x}(t_0) \rightarrow \mathbf{x}(t_0+T_I), \tag{3}$$

since the Lagrangian trajectory of a particle at the position $\mathbf{x}_0$ at time t_0 may be constructed by solving the initial value problem,

$$\frac{d\mathbf{x}}{dt} = \mathbf{u}(\mathbf{x}(t),t), \quad \mathbf{x}(t_0) = \mathbf{x}_0. \tag{4}$$

As in Ref. 25, we define the finite-time version of the right Cauchy–Green deformation tensor,

$$\Delta(\mathbf{x}) = \left(\frac{d}{d\mathbf{x}}\phi_{t_0}^{t_0+T_I}(\mathbf{x})\right)^* \left(\frac{d}{d\mathbf{x}}\phi_{t_0}^{t_0+T_I}(\mathbf{x})\right), \tag{5}$$

and the FTLE field as

$$\sigma_t^{T_I}(\mathbf{x}) = \frac{1}{|T_I|}\log\sqrt{\lambda_{\max}(\Delta(\mathbf{x}))}, \tag{6}$$

where $\lambda_{\max}(\Delta(\mathbf{x}))$ is the maximum eigenvalue of the symmetric matrix $\Delta(\mathbf{x})$ and designates the maximal amount of divergence of fluid particles near $\mathbf{x}$ over the integration time T_I. In order to construct the FTLE field, Lagrangian particle trajectories for an initially seeded array of particles are computed by solving the initial value problem in Eq. (4) using a fourth-order Runge–Kutta scheme. Although the immersed boundary method keeps track of the Eulerian velocity field $\mathbf{u}$ on a grid, one may use the same discrete delta functions used for the full fluid-structure calculations to interpolate velocities from the grid to the Lagrangian particles. The spatial gradients of the flow map needed to assemble the matrix $\lambda_{\max}(\Delta(\mathbf{x}))$ are computed using central differences. We remark that since the stiffness of the internally actuated cilia immersed boundary calculations dictates a small time step (on the order of 10^5 time steps per ciliary beat), we do not evolve the Lagrangian particle tracks at each time step of the full immersed boundary calculation, but evolve their positions in postprocessing, at time intervals of about $\frac{1}{350}$ of a single ciliary beat.

III. RESULTS

A. Cilium-mucus transport

We consider a single cilium of length of 14 μm, emanating from a fixed wall, placed in a square fluid domain whose sides are 40 μm in length. An elastic mucus layer is placed horizontally just above the cilium tip. Periodic boundary conditions on the fluid and the mucus layer are enforced. One may interpret these simulations, then, as portraying an infinite array of cilia, beating in synchrony, transporting an infinitely long mucus layer. Moreover, since the computations are 2D, one may also interpret the simulation in three dimensions (3D) as an infinite array of in-phase ciliary sheets or very closely packed cilia in the direction out of the 2D plane, transporting an infinite mucus surface. Calculations were performed using a 256×256 finite difference grid, and the Lagrangian particles used to assemble the FTLE field were initially launched at these grid locations. Figures 1 and 2 show resulting geometry and positions of the model cilium within the first beat cycle, with an emerging period of $T=0.0256$ s or a beat frequency of about 35 Hz. The simulation was continued for more than eight beat periods, and in what follows we refer to time in units of this beat period T. The Reynolds number of this model cilium, based on ciliary length and ciliary tip velocity, is about 10^{-2}. However, ciliary tip velocity is much larger than typical velocities around the cilium, and the Reynolds number based on ciliary length and mucus transport velocity is about 10^{-3}. These values are in line with the Reynolds number for a cilium in the respiratory tract reported in Ref. 28.

As discussed in Refs. 26 and 33, the choice of an integration time depends on the time scale of the dynamics of interest and should be chosen with respect to a natural scale of the problem, such as beat period. Since the computations presented here assume period boundary conditions on the fluid domain, when a Lagrangian particle is advected out of the computational domain, its periodic copy is introduced back in. Hence, the integration time is not restricted by particles leaving the domain. Figure 3 shows contours of the forward FTLE field at time $t=0$, with different integration times T_I. Visual inspection of the maximal ridges allows us to identify the location of the LCS. Recall that the power stroke of the cilium is toward the right and, hence, the net direction of fluid transport and mucus layer transport is toward the right. Figure 3(a) shows that, with an integration time of one beat period ($T_I=T$), two well-defined ridges appear—one that separates the region of fluid to the right of the cilium from the exterior fluid in the direction of transport and one ridge to the left of cilium, up near the mucus layer.

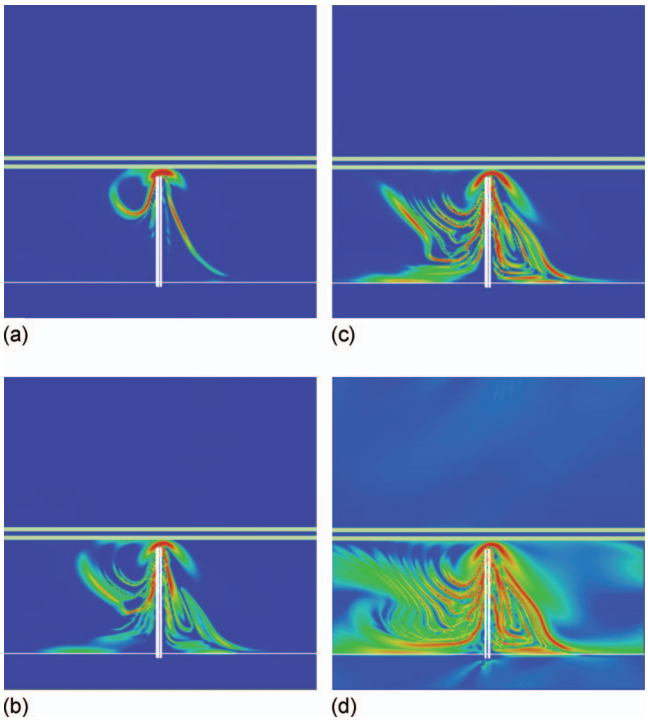

FIG. 3. (Color) Contours of forward-time FTLE field at time $t=0$ for different integration times. Maximal ridges are depicted in red.

With each subsequent beat period added to the integration time, an additional ridge is added to the left of the cilium, and another looped ridge is added within the recirculation region to the right of the cilium (see Fig. 3). Below, we examine the role that these ridges play in fluid transport.

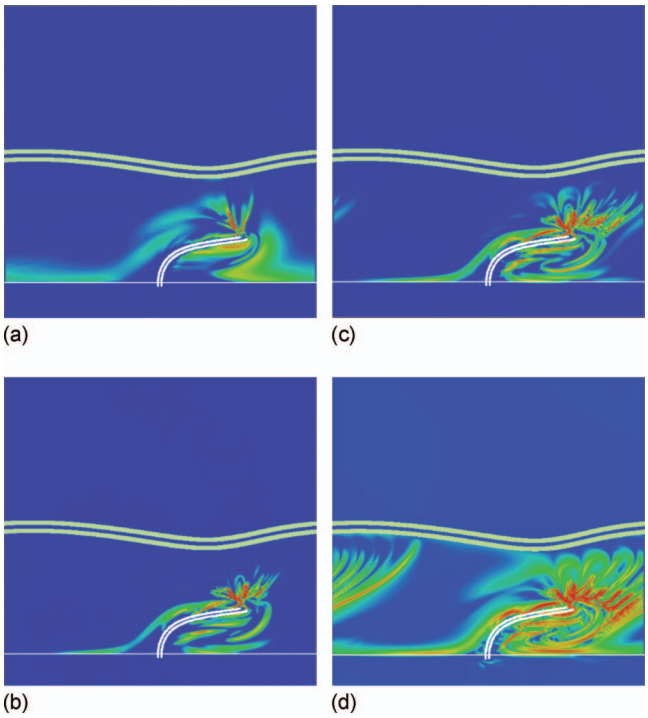

FIG. 4. (Color) Contours of backward-time FTLE field at time $t=8.25T$ for different integration times. Maximal ridges are depicted in red.

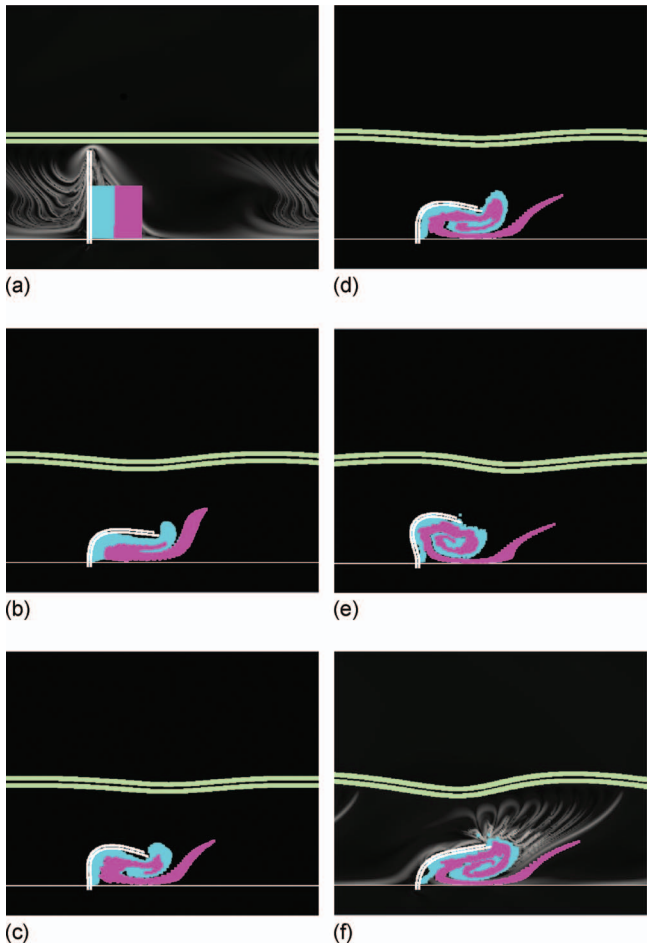

FIG. 5. (Color) Snapshots of cilium, mucus layer, and evolution of a patch of fluid tracer particles initially placed over the recirculation region to the right of the cilium. Frame (a) depicts contours of the forward FTLE field at time $t=0$ using an integration time of $T_I=8.25T$. Frame (f) depicts contours of the backward FTLE field at time $t=8.25T$ using an integration time of $T_I=-8.25T$.

We may also compute the backward FTLE field, by seeding our Lagrangian fluid particles at some time t_1 and using velocity field information to integrate backward in time. Figure 4 shows contours of the backward FTLE field at time $t_1=8.25T$, with different (negative) integration times. Strong corrugated ridges appear emanating from the ciliary tip toward the direction of transport.

In order to investigate the LCS appearing just toward the right of the cilium, we track a densely packed particle patch initially placed over that region [see Fig. 5(a)]. Two very important features emerge. First, there is a definite LCS barrier that separates a recirculation region of fluid near the cilium from fluid that is advected forward. Note that the portion of the pink patch of fluid that initially is above and to the right of the outermost ridge is transported downstream and appears as an extended pink finger toward the right in Fig. 5(f). Second, the region of fluid that stays near the cilium in the recirculation region is not oscillating uniformly, but is periodically stretched and folded, exhibiting mixing reminiscent of a Smale horseshoe map.[32] The asymmetry of the ciliary beat is not only essential for fluid transport but also contributes to fluid mixing. The fluid in the recirculation

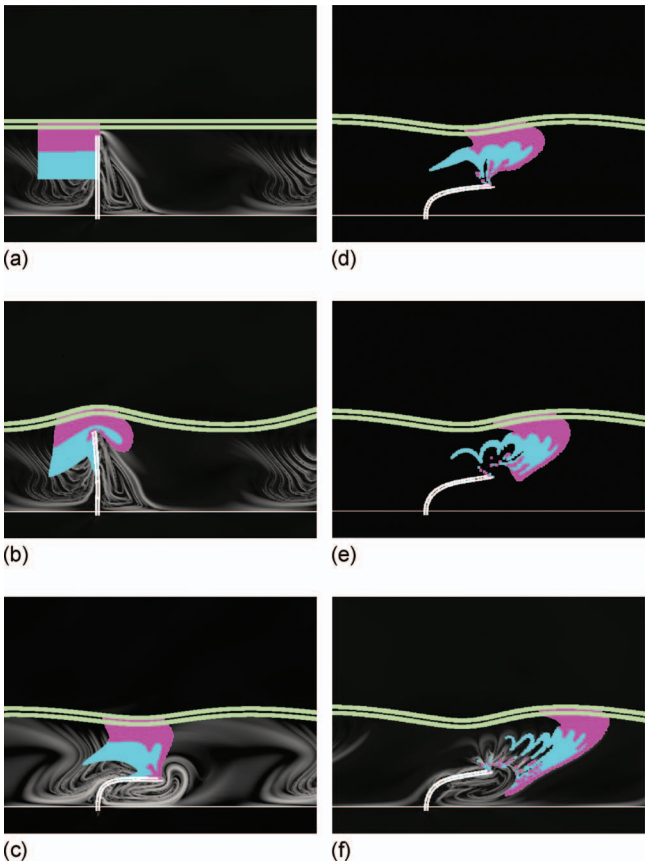

FIG. 6. (Color) Snapshots of cilium, mucus layer, and evolution of a patch of fluid tracer particles initially placed to the left of the cilium extending upward to the mucus layer. Frames (a) and (b) depict contours of the forward FTLE field at time $t=0$ using an integration time of $T_I=8.25T$. Frame (c) depicts contours of the forward FTLE field at time $t=1.25T$ using an integration time of $T_I=7T$. Frame (f) depicts contours of the backward FTLE field at time $t=8.25T$ using an integration time of $T_I=-8.25T$.

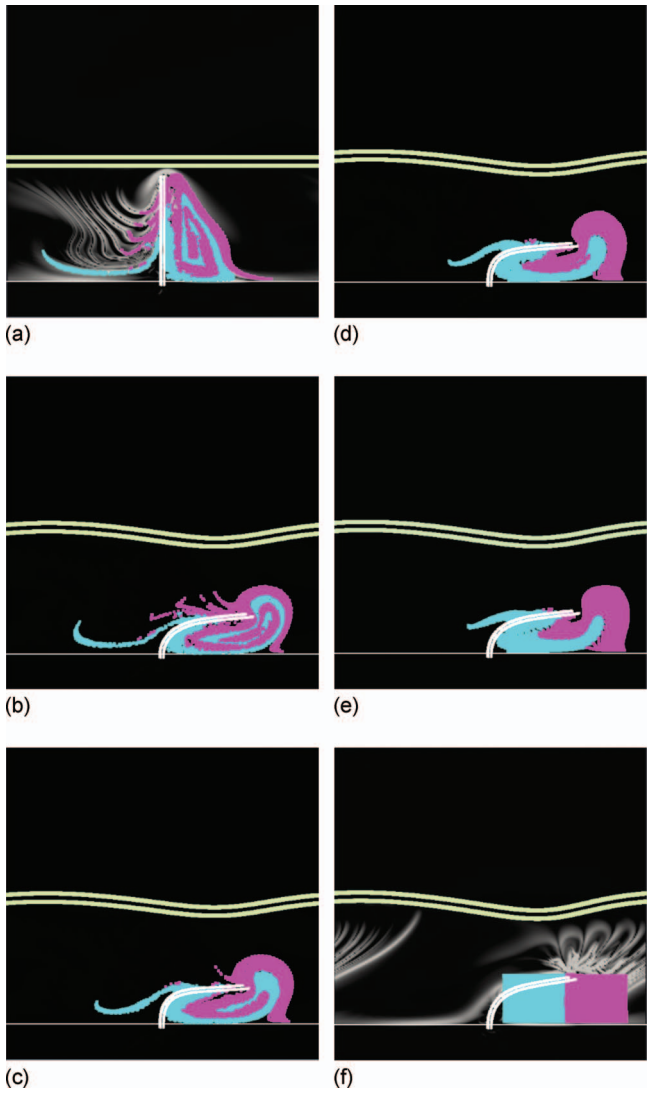

FIG. 7. (Color) Snapshots of cilium, mucus layer, and backward evolution of a patch of fluid tracer particles initially placed overlapping the recirculation region to the right of the cilium and the cilium itself. Frame (a) depicts contours of the forward FTLE field at time $t=0$ using an integration time of $T_I=8.25T$. Frame (f) depicts contours of the backward FTLE field at time $t=8.25T$ using an integration time of $T_I=-8.25T$.

region is stretched as the recovery stroke draws it upward, and then folded as the power stroke pushes it toward the wall. This beautiful evolution of fluid particles is not at all evident by examining Eulerian velocity fields produced by the immersed boundary calculations. Moreover, it would not have been seen by tracking fluid particles of one color in that region—in that case Fig. 5 would have shown a uniform blob of fluid adhered to the cilium. We emphasize that the LCS ridges computed (Fig. 6) uncovered the dynamics of that region.

Next we investigate the LCS appearing toward the left of the cilium, near the mucus layer. We track a densely packed particle patch initially placed over that region [see Fig. 6(a)]. These ridges appearing in the LCS at each beat separate the fluid that makes its way between the cilium and the mucus layer from the fluid that is left behind during that beat. The forward FTLE fields are superimposed in frames [Figs. 6(b) and 6(c)] to show that the fluid that does make it over the cilium does not cross the LCS barrier into the recirculation region. Again, we do see some interesting mixing in the transported fluid patch that would not be evident if all of the tracers were depicted in the same color. Although this model is only a very idealized version of mucus transport in the periciliary layer, we remark that the results of this simulation are consistent with the experimental results of Matsui *et al.*[15] There, it was reported that fluid within the layer is transported uniformly with the mucus layer. However, looking more closely, our simulations show that this is not a plug flow, but within the fluid patch, mixing does occur.

In order to uncover the flow structures suggested by the ridges of the backward FTLE field, we track, backward in time, a densely packed particle patch placed "initially" over that region at time $t_1=8.25T$ (Fig. 7). We see that the "final" locations of these particles in backward time superimpose with the repelling ridges of the forward FTLE field in frame [Fig. 7(a)].

B. Absence of mucus layer

Next we examine how the flow structures and particle fates differ near the beating cilium when the mucus layer is removed. We perform the same simulation as previously, but here extra forces due to a periodic mucus layer are not

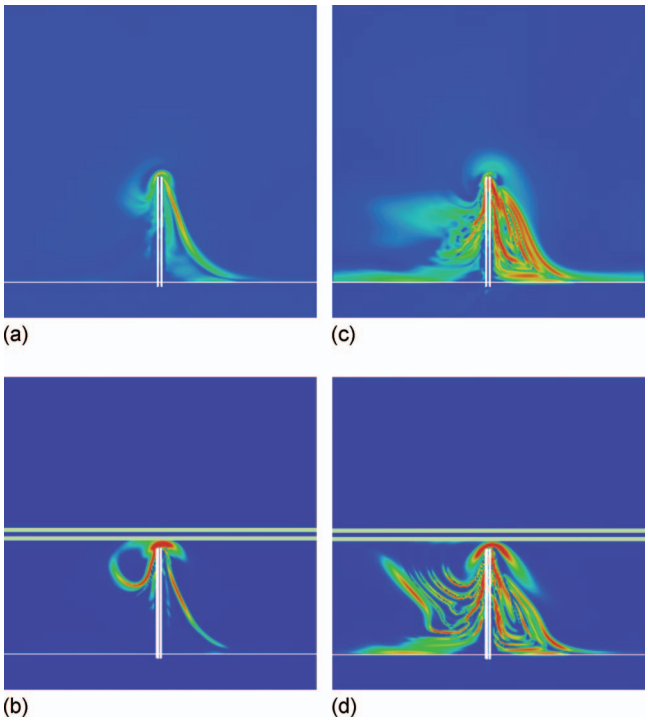

FIG. 8. (Color) Comparison of contours of forward FTLE fields at time $t=0$ between cilium beating with and without mucus layer. Frames (a) and (b) use an integration time of $T_I=T$ and frames (c) and (d) use an integration time of $T_I=5T$.

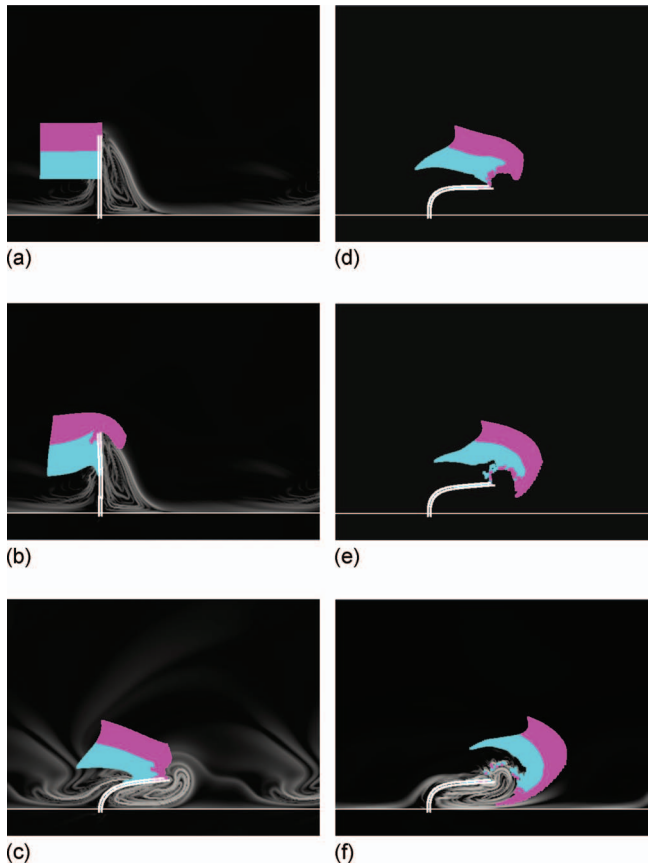

FIG. 9. (Color) Snapshots of cilium and evolution of a patch of fluid tracer particles initially placed to the left of the cilium, as in Fig. 6, but without the presence of the mucus layer. Frames (a) and (b) depict contours of the forward FTLE field at time $t=0$ using an integration time of $T_I=8.25T$. Frame (c) depicts contours of the forward FTLE field at time $t=1.25T$ using an integration time of $T_I=7T$. Frame (f) depicts contours of the backward FTLE field at time $t=8.25T$ using an integration time of $T_I=-8.25T$.

present. We remark that, although there is no added load from the mucus layer, the beat frequency that emerges from this "free" cilium case also turns out to be about 35 Hz, virtually unchanged from the beat frequency of the cilium transporting the mucus layer. We note that this robustness of beat frequency for cilia in tracheobroncial cultures, with or without a mucus layer, was observed in experiments.[15] Figure 8 shows contours of the forward FTLE field at integration times of one and five beat periods for both the mucus and nonmucus cases. In each case, LCS designating a recirculation region to the right of the cilium emerges, as described above. However, the nonmucus case does not give rise to any appreciable ridges on the left of the cilium. Recall that these ridges in the mucus-transporting case corresponded to fluid parcels that were transported between the ciliary tip and the mucus layer. To illustrate this, Fig. 9 tracks a patch of fluid particles to the left of the cilium, analogous to Fig. 6, but without the mucus layer. Again, we see that there is a LCS ridge that acts as a recirculation barrier. However, the transport downstream of the fluid particle patch that is initially placed to the left of the cilium is significantly reduced, and there is less mixing in that patch.

IV. CONCLUSION

In this paper, we analyze flow structures around a computational model of a beating cilium that is propelling a mucus layer. We have shown that the asymmetric power-recovery stroke of a single 2D cilium emanating from a plane wall can propel fluid and mucus forward, but at the same time, generates complex mixing in a recirculation region near the cilium. Previously, dynamical system methods, including examination of local Lyapunov exponents, were used by Otto *et al.*[19] to exhibit rich mixing properties in Stokes flows, by idealizing a ciliary beat by blinking Stokeslets. More recently, a computational study of mixing by pairs of externally actuated cilia was presented by Khatavkar *et al.*[10] The motivation for that study was the potential use of artificial cilia to enhance mixing in microfluidic devices.

We use the Eulerian fluid velocity fields computed by an immersed boundary method to compute LCSs that do reveal intriguing transport and mixing features of the generated flow. Ultimately, we would like to use this methodology to characterize flow structures within the periciliary layer of the airway surface liquid of the lung. Airway cilia are closely packed, may have out-of-plane beats, and exhibit coordinated metachronal waves.[29] Although we present a simple 2D model of an isolated cilium, we have captured some of the complexity of a full cilia-mucus-fluid coupled system. The model cilium is internally actuated, so the beat geometry and frequency emerge from the coupling with the viscous fluid and the elastic mucus layer. Moreover, the transport and deformation of the elastic mucus layer are emergent properties of the coupled system. We view the results presented

here as a promising starting point for future computational analysis of flow features in more comprehensive, 3D models of mucociliary transport.

ACKNOWLEDGMENTS

The computational simulations were performed on the facilities of the Center for Computational Science, Tulane University, and the Louisiana Optical Network Initiative (LONI). The work of S.L. and L.F. was supported in part by NSF DMS Grant No. 0652795. The authors wish to thank John Chrispell and Ricardo Ortiz for their insight and many helpful discussions.

[1]Afzelius, B. A., "Cilia-related diseases," J. Pathol. **204**, 470–477 (2004).
[2]Blake, J. R. and Sleigh, M., "Mechanics of ciliary locomotion," Biol. Rev. Cambridge Philos. Soc. **49**, 85–125 (1974).
[3]Brokaw, C. J., "Simulating the effects of fluid viscosity on the behaviour of sperm flagella," Math. Methods Appl. Sci. **24**, 1351–1366 (2001).
[4]Dillon, R. and Fauci, L., "An integrative model of internal axoneme mechanics and external fluid dynamics in ciliary beating," J. Theor. Biol. **207**, 415–430 (2000).
[5]Dillon, R., Fauci, L., and Omoto, C., "Mathematical modeling of axoneme mechanics and fluid dynamics in ciliary and sperm motility," Dyn. Contin. Discrete Impulsive Syst.: Ser. A - Math. Anal. **10**, 745–758 (2003).
[6]Dillon, R., Fauci, L., Omoto, C., and Yang, X., "Fluid dynamic models of flagellar and ciliary beating," Ann. N.Y. Acad. Sci. **1101**, 494–505 (2007).
[7]Dillon, R. and Othmer, H., "A mathematical model for the outgrowth and spatial patterning of the vertebrate limb bud," J. Theor. Biol. **197**, 295–330 (1999).
[8]Ghosh, A. and Fischer, P., "Controlled propulsion of artificial magnetic nanostructured propellers," Nano Lett. **9**, 2243–2245 (2009).
[9]Haller, G., "Lagrangian structures and the rate of strain in a partition of two-dimensional turbulence," Phys. Fluids **13**, 3365–3385 (2001).
[10]Khatavkar, V., Anderson, P., den Toonder, J., and Meijer, H., "Active micromixer based on artificial cilia," Phys. Fluids **19**, 083605 (2007).
[11]Knowles, M. R. and Boucher, R. C., "Mucus clearance as a primary innate defense mechanism for mammalian airways," J. Clin. Invest. **109**, 571–577 (2002).
[12]Lindemann, C., "A model of flagellar and ciliary functioning which uses the forces transverse to the axoneme as the regulator of dynein activation," Cell Motil. Cytoskeleton **29**, 141–154 (1994).
[13]Marshall, W. and Kintner, C., "Cilia orientation and the fluid mechanics of development," Curr. Opin. Cell Biol. **20**, 48–52 (2008).
[14]Marshall, W. and Nonaka, S., "Cilia: Tuning in to the cell's antenna," Curr. Biol. **16**, R604–R614 (2006).
[15]Matsui, H., Randell, S. H., Peretti, S. W., Davis, C. W., and Boucher, R. C., "Coordinated clearance of periciliary liquid and mucus from airway surfaces," J. Clin. Invest. **102**, 1125–1131 (1998).
[16]Murase, M., *The Dynamics of Cellular Motility* (Wiley, Chichester, 1992).
[17]Nonaka, S., Shiratori, H., Saijoh, Y., and Hamada, H., "Determination of left-right patterning of the mouse embryo by artificial nodal flow," Nature (London) **418**, 96–98 (2002).
[18]Okada, Y., Takeda, S., Tanaka, Y., Belmonte, J., and Hirokawa, N., "Mechanism of nodal flow: A conserved symmetry breaking event in left-right axis determination," Cell **121**, 633–644 (2005).
[19]Otto, S. R., Yannacopoulos, A. N., and Blake, J. R., "Transport and mixing in stokes flow: The effect of chaotic dynamics on the blinking Stokeslet," J. Fluid Mech. **430**, 1–26 (2001).
[20]Peng, J. and Dabiri, J., "An overview of a Lagrangian method for analysis of animal wake dynamics," J. Exp. Biol. **211**, 280–287 (2008).
[21]Peng, J. and Dabiri, J., "The 'upstream wake' of swimming and flying animals and its correlation with propulsive efficiency," J. Exp. Biol. **211**, 2669–2677 (2008).
[22]Peskin, C. S., "The immersed boundary method," Acta Numerica **11**, 479–518 (2002).
[23]Purcell, E. M., "Life at low Reynolds numbers," Am. J. Phys. **45**, 3–11 (1977).
[24]Schweickert, A., Weber, T., Beyer, T., Vick, P., Bogusch, S., Feistel, K., and Blum, M., "Cilia-driven leftward flow determines laterality in xenopus," Curr. Biol. **17**, 60–66 (2007).
[25]Shadden, S., Lekien, F., and Marsden, J., "Definition and properties of Lagrangian coherent structures from finite-time Lyapunov exponents in two-dimensional aperiodic flows," Physica D **212**, 271–304 (2005).
[26]Shadden, S. C. and Taylor, C. A., "Characterization of coherent structures in the cardiovascular system," Ann. Biomed. Eng. **36**, 1152–1162 (2008).
[27]Shah, A., Ben-Shahar, Y., Moninger, T., Kline, J., and Welsh, M., "Motile cilia of human airway epithelia are chemosensory," Science **325**, 1131–1134 (2009).
[28]Sleigh, M. A., Blake, J. R., and Liron, N., "The propulsion of mucus by cilia," Am. Rev. Respir. Dis. **137**, 726–741 (1988).
[29]Smith, D. J., Gaffney, E. A., and Blake, J. R., "Modelling mucociliary clearance," Respir. Physiol. Neurobiol. **163**, 178–188 (2008).
[30]Strathmann, R. and Grunbaum, D., "Good eaters, poor swimmers: Compromises in larval form," Integr. Comp. Biol. **46**, 312–322 (2006).
[31]Talbot, P., Geiske, C., and Knoll, M., "Oocyte pickup by the mammalian oviduct," Mol. Biol. Cell **10**, 5–8 (1999).
[32]Wiggins, S., *Introduction to Applied Nonlinear Dynamical Systems and Chaos* (Springer, New York, 1990).
[33]Wilson, M., Peng, J., Dabiri, J., and Eldredge, J., "Lagrangian coherent structures in low Reynolds number swimming," J. Phys.: Condens. Matter **21**, 204105 (2009).
[34]Witman, G. B., in *Ciliary and Flagellar Membranes*, edited by Bloodgood, R. A. (Plenum, New York, 1990), p. 1.
[35]Yang, X., Dillon, R., and Fauci, L., "An integrative computational model of multiciliary beating," Bull. Math. Biol. **70**, 1192–1215 (2008).